Research Article

INTERNATIONAL JOURNAL OF ADVANCED ROBOTIC SYSTEMS

International Journal of Advanced Robotic Systems
March-April 2018: 1–14

DOI: 10.1177/1729881418765861
journals.sagepub.com/home/arx
SAGE

Relative posture-based kinematic calibration of a 6-RSS parallel robot by optical coordinate measurement machine

Pengcheng Li[1], Rui Zeng[2], Wenfang Xie[1] and Xiaoming Zhang[1]

Abstract

In this article, a relative posture-based algorithm is proposed to solve the kinematic calibration problem of a 6-RSS parallel robot using the optical coordinate measurement machine system. In the research, the relative posture of robot is estimated using the detected pose with respect to the sensor frame through several reflectors which are fixed on the robot end-effector. Based on the relative posture, a calibration algorithm is proposed to determine the optimal error parameters of the robot kinematic model and external parameters introduced by the optical sensor. This method considers both the position and orientation variations and does not need the accurate location information of the detection sensor. The simulation results validate the superiority of the algorithm by comparing with the classic implicit calibration method. And the experimental results demonstrate that the proposal relative posture-based algorithm using optical coordinate measurement machine is an implementable and effective method for the parallel robot calibration.

Keywords

Parallel robot, calibration, optical sensor, kinematic analysis

Date received: 24 December 2017; accepted: 8 February 2018

Topic: Vision Systems
Topic Editor: Andrey V Savkin
Associate Editor: Yongping Pan

Introduction

Parallel robots are closed-loop chain mechanisms whose end-effectors are actuated by a serial of independent computer-controlled serial chains linked to the bases. Parallel robots present some outstanding advantages in high force-to-weight ratio and better stiffness compared with serial manipulators.[1] Hence, parallel robots have been utilized increasingly in various applications such as flight simulators, manufacturing lines, and medical tools.[2]

Normally, the control performance of uncalibrated parallel robots is significantly affected by the manufacturing and robot installation errors. Kinematic calibration is an effective method to remove the negative influence of these errors and to improve the accuracy of end-effector output in a robot control system. The calibration algorithms based on end-effector absolute posture are generally used to determine the optimal robot kinematic model.[3] This kind of algorithm needs accurate absolute location of the robot

[1] Department of Mechanical, Industrial, Aerospace Engineering, Concordia University, Montréal, Canada
[2] Department of Automatic Control, Beihang University, Beijing, People's Republic of China

Corresponding author:
Wenfang Xie, Department of Mechanical, Industrial, Aerospace Engineering, Concordia University, 1455 De Maisonneuve W., Montreal, QC H3G 1M8, Canada.
Email: wfxie@encs.concordia.ca

base frame in the sensor frame through a tedious pre-calibration procedure due to the lack of a well-defined and mechanically accessible base coordinate frame for the robot.[4] The location of the robot base frame with respect to the sensor frame is not needed in the relative posture (or posture variation) calibration. And based on the relative measurement, the constraint equations for deriving the entire considered kinematic parameters of the robot can be constructed for the calibration. Therefore, in this research, we focus on the kinematic model calibration based on robot relative posture with respect to the optical measurement system.

Although some researchers perform the calibration without using a robot kinematic model,[5] most kinematic calibration methods are kinematic model based.[6–8] To identify the error parameters in the robot kinematic model, the model-based calibration is conducted in three steps: modeling, measurement, and calibration.[3]

Based on the geometric analysis, a kinematic error model can be constructed by considering joint residual errors in kinematic parameters. Model-based kinematic calibration tries to rebuild a more accurate mapping between robot actuator outputs and the end-effector posture by determining those kinematic parameters. Precise parallel robot error model is built by denavit-hartenberg (D-H) method.[9] However, most researchers[10,11] choose a reduced model in the calibration considering that the contribution of joint manufacturing tolerances have a minor effect on the platform pose error. In other words, the manufacturing tolerances of the joints are neglectable. Nevertheless, the positional errors of the joint centers and the deviation of the active joint angles are the main reasons for the kinematic calibration.

The measurement sensors play an important role in the parallel robot calibration. It tries to collect enough redundant information for the calibration. The sensors usually fall into two categories: contact measurement and contactless measurement. For the contact measurement type sensors such as translation detector,[12] coordinate measurement machine (CMM),[13] inclinometer,[14] and double ball bar device,[15] they collect various posture information of the robot end-effector directly for the kinematic calibration. However, they have to meet the strict installation requirements. And the installation errors affect the contact measurement results in different directions and with different magnitudes when the measurand is moving. While for the contactless sensors like camera,[10] laser tracker,[16] and optical CMM,[17] it is more flexible to obtain the pose information of the end-effector. The contactless measurement can eliminate the sensor errors with the help of pre-calibration. Alternatively, the sensor location uncertainties can also be viewed as external parameters in terms of the kinematic error model,[10] which may increase the complexity of the error model and the computation cost. Ideally, the detection of relative posture (the variation of robot position and orientation) is independent of the sensors' location. In this article, to realize a flexible installation and to avoid the tedious measurement procedure of the sensor location, an optical CMM sensor C-track 780 from Creaform Inc. (QC, Canada) is adopted to detect the relative pose of the 6-RSS parallel robot.

The classic implicit calibration method proposed in the study by Wampler et al.[18] utilizes the closure relation of the kinematic chains to form implicit constraint equations instead of pursuing the analytical solutions of the closure equations such as the inverse kinematic model. The implicit calibration method emphasizes that the errors are involved in the kinematic loop equations implicitly, rather than being explicit outputs of a conventional input–output formulation.[18] By removing the requirement to express errors explicitly, the formulation allows the analyst to concentrate on all sources of error.[18] And the implicit calibration method has been effectively applied to H4 mechanism10 and 6-UPS robot.[18] In implicit calibration method, the absolute posture of the end-effector with respect to the base frame should be obtained with the employment of the contactless sensor. In most applications, the kinematic calibration is known as an optimization problem with redundant nonlinear constraint equations. The methods such as classical nonlinear algorithms,[9,19] bundle adjustment approach,[20] and interval approach[21] are applied to solve it. The pose vector of end-effector with respect to the base frame is normally used to construct the objective function of the optimization problem based on 2-norm of vector.[10,18,22] Several robot posture configurations should be determined to collect enough information. The principles for the configuration selection of parallel robot calibration have been given in some literature,[23,24] in which the error parameter Jacobian matrix is utilized to minimize the influence of measurement noise in all candidate configurations. For the 6-RSS parallel robot, the effect of the posture selection should be analyzed for relative posture-based algorithm (RPBA).

Most researchers assume the sensor location *is* exactly known in the kinematic calibration experiment.[13,21] Hence, both the absolute and relative postures for the calibration algorithm can be easily determined. However, to derive the pose of the base frame of robots with respect to sensor frame is usually a tedious and time-consuming work due to the following reasons: (1) the manufacturers usually do not provide enough nominal dimension information of the robots and (2) the self-occlusion of the close structure of parallel robots results in measurement difficulties. If the sensor location is not known exactly, the existing absolute posture-based algorithms cannot be used for the kinematic calibration directly. Ideally, the relative posture information, that is, posture variation, can be utilized in the calibration to avoid the tedious measurement of the relationship between the base frame and the sensor frame. A relative position-based calibration algorithm12 is carried out for parallel robots, where a simple measurement system with three distance gauges and a ball mounted on the

end-effector is employed to measure the relative position movement. However, the orientation accuracy cannot be evaluated. Since the gauges should be re-installed with strict rules in every candidate configuration, the installation errors cannot be removed during the calibration.

In this article, we have developed a relative posture-based calibration algorithm for a 6-RSS parallel robot built with a kinematic error model using an optical vision system and several target reflectors attached on the end-effector of the 6-RSS parallel robot. The detected feature points of the reflectors can be used to estimate the relative poses. The obtained relative postures are then used to construct an objective function, and the updating algorithm is determined by minimizing this objective function following the least square norm principle. Simulation has been carried out to prove the superiority of relative pose-based calibration method comparing with the implicit calibration method based on absolute posture measurement. The experimental tests show that the following advantages of the proposed algorithm comparing with the other relative position-based algorithm:12 both the position and orientation variations can be utilized and no accurate location information for the detection sensor is needed. Both simulation and experimental results demonstrate that the proposal RPBA using optical CMM is an implementable and effective method for the parallel robot calibration.

The article is organized as follows. The kinematic error model and the visual detection system are introduced in the section "Kinematic robot model and pose estimation." The section "Calibration algorithm based on optical CMM" presents the classic implicit calibration method and the RPBA based on the optical CMM. In the section "Simulation case study," simulation results on optimal actuator stroke and calibration are presented. Finally, experimental case studies for the 6-RSS parallel robot kinematic calibration are given in the section "Experimental verification," and conclusion is drawn in the last section.

Kinematic robot model and pose estimation

In this section, the kinematic robot error model is built based on the 6-RSS kinematic analysis. And the optical CMM system for the robot posture detection is introduced.

Kinematic modeling and error analysis

The literature survey shows that the research on the actuator-coplanar 6-RSS parallel robot kinematic modeling is very rare. In this research, the kinematic model of the parallel robot is built based on the geometrical analysis. Figure 1 shows the 6-RSS parallel robot with six coplanar rotary actuators. There is only one actuator in each parallel robot chain, and the kinematic model can be described by six equations given as follows

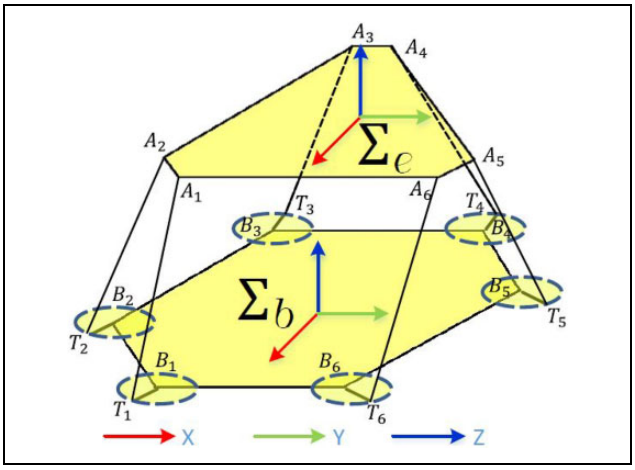

Figure 1. Structure of the 6-RSS parallel robot.

$$l_{A_iT_i} = ||\mathbf{T}_i(\theta_i, l_{T_iB_i}, \mathbf{B}_i) - \mathbf{A}_i({}^b\chi_e, \mathbf{A}'_i)||_2 \quad (i = 1, ..., 6) \tag{1}$$

where $\mathbf{A}_i$ is the coordinate of the ith end-effector terminal expressed in base frame Σb and can be determined by end-effector posture ${}^b\chi_e$ with respect to the base frame and its end-effector frame Σe coordinate $\mathbf{A}'_i$, $\mathbf{T}_i$ is the coordinate of the ith spiral arm terminal with respect to Σb and is determined by actuators' outputs angle θ_i, $\mathbf{B}_i$ is the coordinate of the ith base terminal in Σb frame, and $l_{A_iT_i}$ and $l_{T_iB_i}$ are constant lengths of two arms in the ith chain, respectively. Since the pose (posture) of a certain frame with respect to another frame $\chi = [x, y, z, \beta, \gamma, \alpha]^T$, where (x, y, z) represent the position of the frame origin and (β, γ, α) represents the Euler angle rotation of the frame, can be uniquely represented by the transformation matrix M. In this article, for an arbitrary χ, we have a corresponding symbol M representing its transformation matrix, vice versa. The solved inverse and forward kinematics of the 6-RSS parallel robot can be found in our previous work.[25]

For a complete error modeling of 6-UPS robots, 132 geometric error parameters are identified by Masory et al.[9] The geometric parameters can be reduced to 42 assuming that a good manufacturing quality is applied to the joints. The reduced error model is introduced in Wang's result,[26] which shows that the position accuracy of Stewart platform is insensitive to the joint errors. The reduced kinematic error model is considered in this article. Notice that the joint values θ_i are measured by built-in potentiometers in the 6-RSS parallel robot. The linear relationship

$$\theta_i = \eta_i\kappa_i + \Delta\theta_i \quad (i = 1, ..., 6) \tag{2}$$

between the angle offset $\Delta\theta_i$, sensor outputs κ_i, and angle conversion coefficients η_i can be used to compute θ_i.[27] Based on the kinematic analysis, the considered parameters include initial terminal coordinate errors $\Delta\mathbf{A}'_i = [\Delta x'_{ai}, \Delta y'_{ai}, \Delta z'_{ai}]^T$, $\Delta\mathbf{B}_i = [\Delta x_{bi}, \Delta y_{bi}, \Delta z_{bi}]^T$; length errors $\Delta l_{A_iT_i}$, $\Delta l_{T_iB_i}$; angle

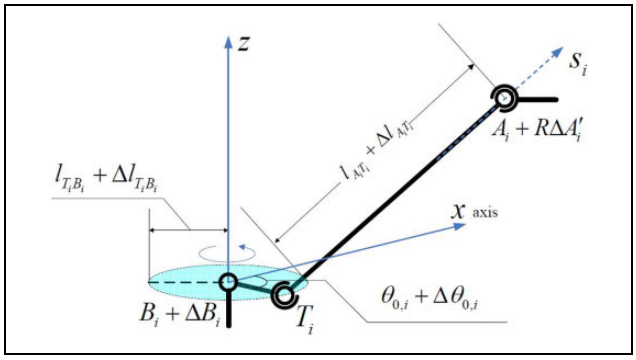

Figure 2. Error parameters considered in the model.

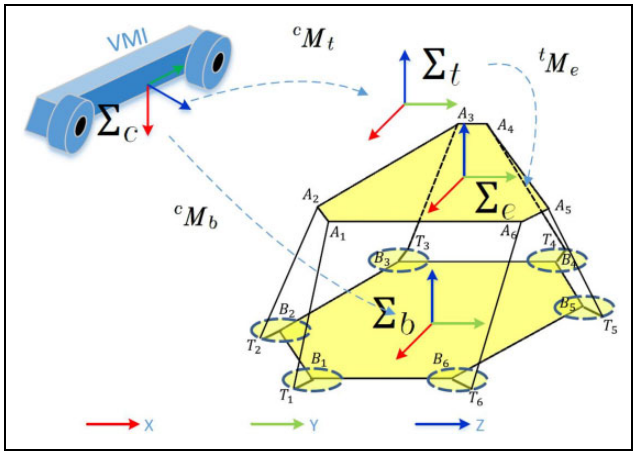

Figure 3. The calibration system of 6-RSS parallel robot.

conversion coefficients η_i; and angle offset $\Delta\theta_i$, where $i = 1, 2, ..., 6$. Figure 2 shows the kinematic structure of the ith chain for the parallel robot with errors marked. Hence, 60 unknown parameters are considered in the kinematic model. And those parameters are denoted as the column vector

$$\begin{aligned}\mathbf{b}_k = [&\Delta x'_{a1}; \Delta y'_{a1}; \Delta z'_{a1}; \ldots; \Delta x'_{a6}; \Delta y'_{a6}; \Delta z'_{a6};\\ &\Delta x_{b1}; \Delta y_{b1}; \Delta z_{b1}; \ldots; \Delta x_{b6}; \Delta y_{b6}; \Delta z_{b6};\\ &\Delta l_{A_1T_1}; \ldots; \nu l_{A_6T_6}; \Delta l_{T_1B_1}; \ldots; \Delta l_{T_6B_6};\\ &\eta_1; \ldots; \eta_6; \Delta\theta_1; \ldots; \Delta\theta_6] = [b_1, b_2, \ldots b_{60}]^T.\end{aligned}$$

The kinematic error model is then given as follows

$$\begin{aligned}l_{A_iT_i} + \Delta l_{A_iT_i} = \| \mathbf{T}_i(\eta_i\kappa_i + \Delta\theta_i, l_{T_iB_i} + \Delta l_{T_iB_i}, \mathbf{B}_i + \Delta\mathbf{B}_i)\\ -\mathbf{A}_i({}^b\chi_e, \mathbf{A}'_i + \Delta\mathbf{A}'_i)\|_2 \quad (i = 1, ..., 6)\end{aligned} \tag{3}$$

Pose estimation using optical CMM

The kinematic calibration can be converted to an optimization problem with redundant nonlinear constraint equations. As shown in Figure 3, a dual-camera optical CMM C-track 780 is employed to estimate the pose of end-effector as redundant data for the optimization problem in this research. The pose estimation principle of binocular vision is presented in this subsection. n reflectors ($n > 3$) placed on the robot are chosen as feature points to form the target frame Σt. Given a group of noncollinear feature points $p_i\,(i = 1, 2, ..., n)$, whose homogeneous coordinates values in the sensor frame are denoted by ${}^C\mathbf{P}_i = [x_{pi}, y_{pi}, z_{pi}, 1]^T$, the relative posture ${}^c\chi_t$ between the target frame and the sensor frame ΣC can be estimated. The projection coordinates of ${}^C\mathbf{P}_i$ on the image frame of each camera can be written as ${}^I\mathbf{P}_{ij} = (u_{ij}, v_{ij}, 1)$, $i = 1 \cdots n$, and $j = 1, 2$, where j is the number of dual cameras. ${}^I\mathbf{W}_j$ is the projection matrix of each camera. The perspective projection can be given as follows[28]

$${}^I\mathbf{P}_{ij} = {}^I\mathbf{W}_j{}^C\mathbf{P}_i\,, {}^I\mathbf{W}_j = \mathbf{B}_j{}^I\mathbf{M}_{Cj} \tag{4}$$

where $\mathbf{B}_j$ is the camera matrix, including the intrinsic parameters of the jth camera; ${}^I\mathbf{M}_{Cj}$ is the homogeneous transformation matrix from the sensor frame ΣC to the jth image frame; and $\mathbf{B}_j$ and ${}^I\mathbf{M}_{Cj}$ can be derived through calibration of the optical sensor. Due to the lens distortion, calibration errors, and other uncertainties, the ${}^C\mathbf{P}_i$ derived from each camera is different. The triangulation is the main way to balance the difference in the results.[29] In order to ensure a matching pair of points, ${}^I\mathbf{P}_{i1}$ and ${}^I\mathbf{P}_{i2}$, meet in space, the following constraint should be satisfied

$${}^I\mathbf{P}_{i1}^T\,\mathbf{G}{}^I\mathbf{P}_{i2} = 0, \tag{5}$$

where $\mathbf{G}$ is the fundamental matrix that can be computed when dual camera projection matrices, ${}^I\mathbf{M}_1$ and ${}^I\mathbf{M}_2$, are given. Due to the uncertainty of image processing, equation (5) may not be satisfied accurately. According to the optimal correction principle of Kanatani et al.,[30] the objective function is

$$\min_{{}^C\mathbf{P}_{i1}{}^T\mathbf{G}{}^C\mathbf{P}_{i2}=0} \left(d\left({}^C\mathbf{P}_{i1}, {}^C\hat{\mathbf{P}}_{i1}\right) + d\left({}^C\mathbf{P}_{i2}, {}^C\hat{\mathbf{P}}_{i2}\right)\right) \tag{6}$$

where $\min(\cdot)$ represents the minimization function subject to the constraint ${}^C\hat{\mathbf{P}}_{i1}{}^T\mathbf{G}{}^C\hat{\mathbf{P}}_{i2} = 0$, $d(*, *)$ denotes Euclidean distance, and ${}^C\hat{\mathbf{P}}_{i1}$ and ${}^C\hat{\mathbf{P}}_{i2}$ are the estimated points of ${}^C\mathbf{P}_{i1}$ and ${}^C\mathbf{P}_{i2}$, respectively. As a result, ${}^C\hat{\mathbf{P}}_{i1}$ and ${}^C\hat{\mathbf{P}}_{i2}$ can be derived. Then, by equation (4), the coordinate of the ith feature point in sensor frame, ${}^C\mathbf{P}_i$, can be obtained.

After the position information of all the feature points on the end-effector is prepared, the pose estimation of the end-effector can be developed. Suppose n feature points on the rigid end-effector are fixed and known from the definition of the tool frame Σt, whose homogeneous coordinates are denoted as ${}^t\mathbf{P}_i = ({}^tx_i, {}^ty_i, {}^tz_i, 1)$. It is assumed the current pose of Σt in the sensor frame ΣC is denoted as ${}^t\chi_c$. Correspondingly, the transformation equation of the ith feature point can be written as

$${}^C\mathbf{P}_i = {}^C\mathbf{M}_t{}^t\mathbf{P}_i \tag{7}$$

where ${}^C\mathbf{M}_t$ is the homogeneous transformation matrix from Σt to ΣC. In order to derive ${}^C\mathbf{M}_t$, at least three noncollinear

feature points are required.[31] However, as indicated in the study by Yuan,[32] at least four coplanar feature points are necessary for a unique solution, while additional noncoplanar feature points can be used to improve the estimation accuracy with measurement noise. Using the proprietary software VXelements provided by Creaform, the target frame can be defined based on the selected reflectors on the surface of the end-effector. The positional and rotational information of the target frame with respect to sensor frame can be acquired, recorded, or displayed simultaneously. Therefore, the computation to obtain the pose of the target frame is carried out by VXelements.

Calibration algorithm based on optical CMM

In this section, we start with the classical implicit calibration method based on optical CMM for parallel robots. Since optical CMM device is involved, external parameters that describe the relationships between base frame and device frame, end-effector frame and target frame should be considered during the implementation of this method. The kinematic parameter $\mathbf{b}_k$ can be seen as the internal parameters. Then we propose a RPBA for parallel robot calibration based on optical devices. It can be seen that less external parameters are needed in RPBA. Then the constraints for candidate configurations selection are determined. Finally, the identifiability and observability analysis of the calibration is given for both calibration methods.

Implicit calibration based on optical CMM

The implicit kinematic model that depicts the closed structure of parallel robots is commonly employed in parallel robots kinematic calibration, since it can avoid solving inverse kinematics and forward kinematics.[18] The choice of implicit kinematic model can be various. Normally, it should be equations that reflect the relationships between joint values, kinematic parameters, and the pose of end-effector. For the 6-RSS parallel robot, the constraint equations Φ_I of implicit kinematic model for calibration can be derived from equation (3)

$$\begin{aligned}\Phi_{Ii}(\mathbf{b}_k, \kappa_i, {}^bM_e) = \| \, & \mathbf{T}_i(\eta_i\kappa_i + \Delta\theta_i, l_{T_iB_i} + \Delta l_{T_iB_i}, \mathbf{B}_i + \Delta\mathbf{B}_i) \\ & - \mathbf{A}_i({}^bM_e, \mathbf{A}'_i + \Delta\mathbf{A}'_i)\|_2 - (l_{A_iT_i} + \Delta l_{A_iT_i}) \\ & = 0 \quad (i = 1, ..., 6)\end{aligned} \tag{8}$$

where Φ_{Ii} is the ith element of Φ_I. Then the kinematic calibration can be derived by solving an optimization problem with the measurement of joint values κ_i^l and postures ${}^b\chi_e^l$ at the lth candidate configuration, and the total number m of candidate configurations should satisfy $6m > 60$. The cost functions for calibration can be written as follows

$$\min_{\mathbf{b}_k} \sum_{l=1}^{m}\sum_{i=1}^{6} \| \, \Phi_{Ii}\left(\mathbf{b}_k, \, \kappa_i^l, \, {}^bM_e^l\right) \, \|_2^2 \quad (i = 1, ..., 6) \tag{9}$$

However, due to the employment of an external optical device, ${}^b\chi_e$ cannot be achieved directly, since one shall take the pose of the sensor frame ${}^b\chi_c$ with respect to the base frame of the parallel robot and the pose of the target frame ${}^e\chi_t$ with respect to the end-effector frame into account. The homogeneous transformation matrices corresponding to ${}^b\chi_c$ and ${}^e\chi_t$ is ${}^bM_c$ and ${}^eM_t$, respectively. Then ${}^bM_e^l$ can be derived from the following equation[10]

$${}^bM_e^l = {}^bM_c \, {}^cM_t^l \, {}^tM_e \tag{10}$$

where ${}^cM_t^l$ represents the measurement of target frame pose related to the camera frame at the l th calibration configuration and ${}^tM_e = {}^eM_t^{-1}$.

The 12 parameters representing ${}^b\chi_c = [{}^bx_c, {}^by_c, {}^bz_c, {}^b\beta_c, {}^b\gamma_c, {}^b\alpha_c]^T$ and ${}^t\chi_e = [{}^tx_e, {}^ty_e, {}^tz_e, {}^t\beta_e, {}^t\gamma_e, {}^t\alpha_e]^T$ can be viewed as the external parameters for the implicit calibration of parallel robots based on the optical CMM sensor, written as a column vector $\mathbf{b}_{Ie} = [{}^bx_c, {}^by_c, {}^bz_c, {}^b\beta_c, {}^b\gamma_c, {}^b\alpha_c, {}^tx_e, {}^ty_e, {}^tz_e, {}^t\beta_e, {}^t\gamma_e, {}^t\alpha_e]^T$. Then substituting equation (10) into equation (9), the cost function becomes

$$\min_{\mathbf{b}_k, \mathbf{b}_{Ie}} \sum_{l=1}^{m}\sum_{i=1}^{6} \| \, \Phi_{Ii}(\mathbf{b}_k, \, \mathbf{b}_{Ie}, \kappa_i^l, \, {}^cM_t^l) \, \|_2^2 \tag{11}$$

Then the updating formula for $\mathbf{b}_I = [\mathbf{b}_k; \mathbf{b}_{Ie}]$ is given as follows

$$\mathbf{b}_I^{t+1} = (J_I^T J_I)^{-1} J_I^T \Phi_I^t + \mathbf{b}_I^t \tag{12}$$

where $\mathbf{b}_I^t$, Φ_I^t is the value of $\mathbf{b}_I$, Φ_I in the t th iteration, respectively and J_I is the Jacobian matrix of Φ_I about $\mathbf{b}_I$ as given in the following equation

$$J_I = \begin{bmatrix} \dfrac{\partial\Phi_I^1}{b_{I1}} & \dfrac{\partial\Phi_I^1}{b_{I2}} & \cdots & \dfrac{\partial\Phi_I^1}{b_{I72}} \\ \dfrac{\partial\Phi_I^2}{\partial b_{I1}} & \dfrac{\partial\Phi_I^2}{\partial b_{I2}} & \cdots & \dfrac{\partial\Phi_I^2}{\partial b_{I72}} \\ \vdots & \vdots & \cdots & \vdots \\ \dfrac{\partial\Phi_I^m}{\partial b_{I1}} & \dfrac{\partial\Phi_I^m}{\partial b_{I2}} & \cdots & \dfrac{\partial\Phi_I^m}{\partial b_{I72}} \end{bmatrix} \tag{13}$$

In some researches,[33,34] the vector $\mathbf{b}_{Ie}$ is derived from hand-eye calibration and calibrated independently, assuming the calibration of kinematic parameters is well carried out. But in our case, the $\mathbf{b}_{Ie}$ appears in every constraint equation, the calibration of $\mathbf{b}_k$ and $\mathbf{b}_{Ie}$ should be calculated simultaneously.

To achieve the better results in solving the nonlinear optimization problem, accurate initial guesses of $\mathbf{b}_k$ and $\mathbf{b}_{Ie}$ are needed. For $\mathbf{b}_k$, the nominal values provided by

manufacturer of parallel robots can be used as the initial guess. However, the initial guess of $\mathbf{b_e}$ should be measured manually. Taking the advantages of optical CMM sensor, the ${}^{t}\chi_{e}$ can be observed and computed easily. However, due to the lack of a well-defined and mechanically accessible base frame for the parallel robots, the process of deriving the transformation matrix from the optical sensor frame to the base frame can be expensive and time-consuming. If the ${}^{c}\chi_{b}$ can only be roughly measured, this may lead to unhealthy results of $\mathbf{b}_k$ from the nonlinear optimization.

RPBA based on optical CMM

Here we propose RPBA in which the posture variation of parallel robot end-effector can be used to eliminate the influence of external parameters. The transformation matrix M^l expressing the relative pose between the lth end-effector configuration ${}^{c}\chi_{t}^{l}$ and an arbitrarily initial pose ${}^{c}\chi_{t}^{0}$ obtained from optical sensor can be derived as follows

$$M^l = {}^{c}M_{t}^{0\,-1}\ {}^{c}M_{t}^{l} \tag{14}$$

The forward kinematic of the 6-RSS parallel robot can be represented by $g : W \rightarrow \mathrm{SE}(3), \theta = f({}^{b}M_{e})$, W is the actuator parameter space. Then the transformation matrix of initial posture ${}^{b}M_{e}^{0}$ and the lth configuration ${}^{b}M_{e}^{l}$ is determined as ${}^{b}M_{e}^{0} = f(\theta_0)$ and ${}^{b}M_{e}^{l} = f(\theta_l)$, respectively, if the forward function of f exists in the posture ${}^{b}\chi_{e}^{0}$ and ${}^{b}\chi_{e}^{l}$. The transformation matrix M^l of the relative pose can also be obtained by

$$M^l = ({}^{c}M_{b}\,{}^{b}M_{e}^{0}\,{}^{e}M_{t})^{-1}\,{}^{c}M_{b}\,{}^{b}M_{e}^{l}\,{}^{e}M_{t} = {}^{e}M_{t}^{-1}\,{}^{b}M_{e}^{0\,-1}\,{}^{b}M_{e}^{l}\,{}^{e}M_{t} \tag{15}$$

If we define the bijective mapping from homogeneous transformation matrix to the posture as $\chi = L(M)$, combining equations (14) and (15), the constraint function Φ_R for calibration can be derived as the following equations

$$\begin{aligned} &\Phi_R(\mathbf{b}_k, \mathbf{b}_{Re}, \kappa^0, \kappa^l, {}^{c}M_{t}^{0}, {}^{c}M_{t}^{l}) = L({}^{c}M_{t}^{0\,-1}\ {}^{c}M_{t}^{l}) \\ &- L({}^{e}M_{t}^{-1}\,{}^{b}M_{e}^{0\,-1}\,{}^{b}M_{e}^{l}\,{}^{e}M_{t}) = L({}^{c}M_{t}^{0\,-1}\ {}^{c}M_{t}^{l}) \\ &- L({}^{e}M_{t}^{-1} f(\kappa^0, \mathbf{b}_k)^{-1} f(\kappa^l, \mathbf{b}_k)\,{}^{e}M_{t}) = \mathbf{0} \end{aligned} \tag{16}$$

where $\Phi_R(\mathbf{b}_k, \mathbf{b}_{Re}, \kappa^0, \kappa^l, {}^{c}M_{t}^{0}, {}^{c}M_{t}^{l})$ is a 6×1 vector, $\kappa^0 = [\kappa_1^0, \kappa_2^0, \ldots, \kappa_6^0]^T$, $\kappa^l = [\kappa_1^l, \kappa_2^l, \ldots, \kappa_6^l]^T$ can be obtained from potentiometers, and ${}^{c}M_{t}^{0}, {}^{c}M_{t}^{l}$ are measured by the optical sensor. The external parameters for the relative calibration method $\mathbf{b}_{Re} = [{}^{t}x_e, {}^{t}y_e, {}^{t}z_e, {}^{t}\beta_e, {}^{t}\gamma_e, {}^{t}\alpha_e]^T$ are just about the six parameters from ${}^{e}\chi_{t}$. Based on the classical nonlinear least square method and the forward kinematic, an objective function for the kinematic calibration is defined as follows

$$\min_{\mathbf{b}_R} \sum_{l=1}^{m} \parallel \Phi_R(\mathbf{b}_R, \kappa^0, \kappa^l, {}^{c}M_{t}^{0}, {}^{c}M_{t}^{l}) \parallel_{2}^{2} \tag{17}$$

where $\mathbf{b}_R = [\mathbf{b}_k; \mathbf{b}_{Re}]$. Then the updating formula for $\mathbf{b}$ is given as follows

$$\mathbf{b}_R^{t+1} = (J_R^T J_R)^{-1} J_R^T\, \Phi_R^t + \mathbf{b}_R^t \tag{18}$$

where $\mathbf{b}_R^t$ is the value of $\mathbf{b}_R$ in the tth iteration and J_R is the Jacobian matrix of Φ_R about $\mathbf{b}_R$ as given in the following equation

$$J_R = \begin{bmatrix} \frac{\partial \Phi_R^1}{\partial \mathbf{b}_{R1}} & \frac{\partial \Phi_R^1}{\partial \mathbf{b}_{R2}} & \cdots & \frac{\partial \Phi_R^1}{\partial \mathbf{b}_{R66}} \\ \frac{\partial \Phi_R^2}{\partial \mathbf{b}_{R1}} & \frac{\partial \Phi_R^2}{\partial \mathbf{b}_{R2}} & \cdots & \frac{\partial \Phi_R^2}{\partial \mathbf{b}_{R66}} \\ \vdots & \vdots & \cdots & \vdots \\ \frac{\partial \Phi_R^m}{\partial \mathbf{b}_{R1}} & \frac{\partial \Phi_R^m}{\partial \mathbf{b}_{R2}} & \cdots & \frac{\partial \Phi_R^m}{\partial \mathbf{b}_{R66}} \end{bmatrix} \tag{19}$$

As we can see from equation (17), the parameters representing ${}^{c}M_{b}$ which lie in $\mathbf{b}_I e$ are omitted in the relative calibration method and only the parameters involved in ${}^{e}M_{t}$ which can be easily calibrated using optical sensor are needed in this method.

Constraints determination for robot configuration selection

The robot configurations used in the kinematic calibration, or named as candidate configurations, will affect the performance of calibration results.[24] In this section, we first introduce the constraints for the robot configurations selection based on kinematic analysis results on workspace and singularity.[25] According to the updating formula (12), two constraints for the candidate configuration selection are listed as follows:

1. They should be selected in a workspace where any robot configuration corresponds to unique actuator outputs.
2. The kinematic mapping f is totally singularity-free so that all elements in J_T exist.

The first constraint, known as homomorphism constraint,[35] ensures that the forward and the inverse kinematic calculation will converge to the right value during the calibration. Based on the implicit function theorem, the existence of all elements in J_T requires for the singularity-free of inverse kinematic mapping. As the Euler angles are limited in $[-\pi, \pi]$, the mapping h is a homomorphism which ensures that the forward and the inverse kinematic mapping have the same kind of geometric characteristic. Then for the second constraint, we require a singularity-free f. The singularity analysis is normally based on the Jacobian matrix of the kinematic mapping.[36] As shown in Figure 1, when the velocity projection of A_i and T_i on A_iT_i equals each other, we have the following equation

$$s_i^T \cdot \dot{\theta}_i \cdot l_{T_iB_i} \cdot sw_i = s_i^T \cdot (v_{o'} + \omega_{o'} \times A_i) \tag{20}$$

where $i = 1, \ldots, 6$, s_i is the velocity unit vector for A_iT_i, sw_i is the velocity unit vector for terminal T_i, and $v_{o'}$ and $\omega_{o'}$ are the translational velocity vector and angular velocity vector of Σe with respect to the base frame, respectively. Then equation (20) can be represented by the following equation

$$J_1\dot{\theta} = J_2\begin{bmatrix} v_{o'} \\ \omega_{o'} \end{bmatrix} \tag{21}$$

where

$$J_1 = \operatorname{diag}(s_1^T sw_1 l_{T_1B_1}, s_2^T sw_2 l_{T_2B_2}, ..., s_6^T sw_6 l_{T_6B_6})$$

$$J_2 = \begin{bmatrix} s_1^T & (A_1 \times s_1)^T \\ \vdots & \vdots \\ s_6^T & (A_6 \times s_6)^T \end{bmatrix}$$

As shown in the study by Park and Kim,[36] if $\det(J_1) = 0$, type I singularity occurs and the 6-RSS parallel robot meets its boundary of available workspace. If all the diagonal elements of J_1 hold their signs in a workspace, the parallel robot stays in a type I singularity-free range. The robot type II singularity of 6-RSS parallel robot occurs when $\det(J_2) = 0$. To avoid the perturbation from the degenerated singularity surface, the Cauchy index ∇ of J_2 can be used to identify the type II singularity.[35] For any two nearby points $p_1, p_2 \in M$:

1. If $|\nabla_{p_1}^{J_2} - \nabla_{p_2}^{J_2}| = 0$, line p_1p_2 stays in a type II singularity-free domain.
2. If $|\nabla_{p_1}^{J_2} - \nabla_{p_2}^{J_2}| = 2$, line p_1p_2 crosses a nondegenerate type II singularity surface.
3. If $|\nabla_{p_1}^{J_2} - \nabla_{p_2}^{J_2}| > 2$ and $\min_{p_1p_2} \det(J_2) = 0$, line p_1p_2 crosses a degenerated type- II singularity surface.

Singularity-free is not a sufficient condition for the uniqueness of forward kinematic solution in parallel robots.[37] The second constraint requires for a workspace in which f is a bijective mapping. The conclusion in our previous study[35] is directly used: kinematic mapping f is a homeomorphism if the following equation holds:

$$\sqrt[\frac{2}{n}]{\sum_{i=1}^{n}\sigma_i^2} \le C \cdot \left|\prod_{i=1}^{n}\lambda_i\right| \tag{22}$$

where σ_i and λ_i are the ith singular value and the eigenvalue of $J_a = J_2^{-1}J_1$, respectively and $C \ge 1$ is a bounded real number.

Identifiability and observability index

Since external parameters are involved in both implicit calibration and relative calibration, we first need to check the identifiability of external parameters and kinematic parameters to see if there is linear dependency between those parameters. According to equations (13) and (19), if any parameter did not lie in the kernel of the regressor J_I and J_R, the parameter to be calibrated cannot be updated in each iteration, which means the parameter is non-identifiable. Therefore, the full rank of J_I and J_R should be guaranteed.

In addition to checking the identifiability of kinematic and external parameters, the observability should also be considered to minimize the estimation errors by selecting an optimal set of calibration candidate configurations. In this research, the observability index proposed in the study by Borm and Meng,[38] which emphasizes the volume of a hyper-ellipsoid whose directions are represented by the singular values denoted by $\sigma_1 \ge \sigma_2 \ge \cdots \ge \sigma_w$, is chosen as the criteria in this research. The index O can be expressed as (take J_I case for instance)

$$O = \frac{\sqrt[w]{\sigma_1\sigma_2\cdots\sigma_w}}{\sqrt{m}} = \frac{\sqrt[w]{\det\left(\sqrt{J_I^T J_I}\right)}}{\sqrt{m}} \tag{23}$$

where m is the number of calibration candidate configurations and w is the number of error parameters.

Simulation case study

In this section, simulations are based on the geometry of 6-RSS parallel robot depicted in Figure 1 and the setup is shown in Figure 3. We firstly determine the proper actuator strokes for RPBA. And the optimal set of candidate configurations is determined for both implicit and relative calibration method. Then the calibration simulation comparison of two calibration methods is implemented to show the superiority of RPBA.

The actuator stroke for calibration posture determination

Compared with the end-effector postures, it is more convenient to describe the robot configuration by the actuator joints value. Hence, the results in this subsection are all determined in the actuator parameter space. Besides, the kinematic calculation is based on ideal kinematic model. Two kinds of parallel robot configurations should be detected for the kinematic calibration: the initial configuration and the candidate configurations. The optimal initial actuator angles should be $[-60^\circ, -60^\circ, 180^\circ, 180^\circ, 60^\circ, 60^\circ]$ regarding to our previous work.[25] For the selection of candidate postures, we try to determine the maximum singularity-free actuator stroke in which the kinematic equation f is a homomorphism mapping. Considering the symmetric structure of the 6-RSS parallel robot, the optimization problem can be simplified into a single-objective planning: finding the maximum of actuator strokes under constraint conditions introduced in the last section. The used constraint conditions and parameters are listed as follows:[25]

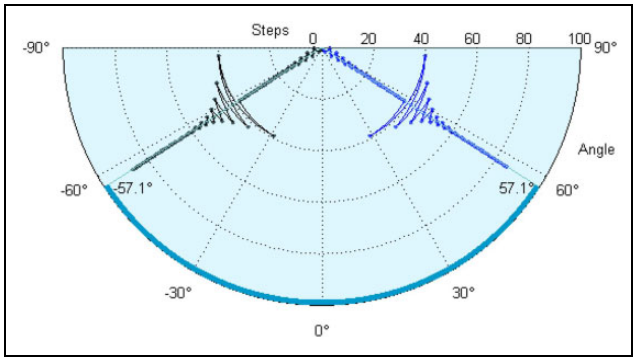

Figure 4. The determination of proper actuator stroke.

1. initial angles $[-60°, -60°, 180°, 180°, 60°, 60°]$;
2. singularity I-free condition $\text{sgn}(J_1) = [+, -, +, -, +, -]$;
3. singularity II-free condition $\Delta^{J_2} = 0$ and $\det(J_2) \neq 0$; and
4. homomorphism condition equation (22).

The optimization procedure is shown in Figure 4. Assuming the initial angle is at the zero degree axis of the polar coordinate, we try to determine the upper and lower bounds of the actuator stroke. In the first 40th step, the two bounds are modified together. After the 40th step, the two bounds are modified separately. Finally, the robot configurations should be selected in the actuator stroke $(-57.1°, 57.1°)$. We verify the homomorphism constraint in the boundaries of the determined actuator stroke to ensure the uniqueness of inverse and forward kinematic solution. The searching trajectory starts from initial angles and is determined by link terminal points of the actuator strokes. Because the trajectory is selected from the boundary of the maximum singularity-free domain, as shown in Figure 5, the value of $\det(J_a)$ is almost zero in every point of the trajectory. From equation (22), as the value of C is bounded, the kinematic function f is a bijective (homomorphism) mapping in the determined actuator stroke.

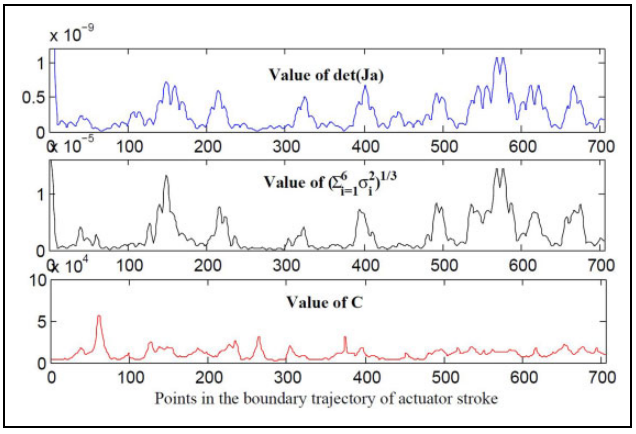

Figure 5. Bijective verification through the boundaries.

Optimal set of calibration configurations selection simulation

In this subsection, we check the identifiability and the observability of the kinematic parameters for both implicit calibration and relative calibration. According to the section "Identifiability and observability index," the identifiability of $\mathbf{b}_I$ and $\mathbf{b}_R$ in both calibration methods is dependent on the Jacobian matrix j_I and j_R which are calculated numerically (take the relative method case for instance) as

$$J_R = \begin{bmatrix} \dfrac{\Phi_R^1(b_{R1}+\varepsilon)-\Phi_R^1}{\varepsilon} & \dfrac{\Phi_R^1(b_{R2}+\varepsilon)-\Phi_R^1}{\varepsilon} & \cdots & \dfrac{\Phi_R^1(b_{R66}+\varepsilon)-\Phi_R^1}{\varepsilon} \\ \dfrac{\Phi_R^2(b_{R1}+\varepsilon)-\Phi_R^2}{\varepsilon} & \dfrac{\Phi_R^2(b_{R2}+\varepsilon)-\Phi_R^2}{\varepsilon} & \cdots & \dfrac{\Phi_R^2(b_{R66}+\varepsilon)-\Phi_R^2}{\varepsilon} \\ \vdots & \vdots & \cdots & \vdots \\ \dfrac{\Phi_R^m(b_{R1}+\varepsilon)-\Phi_R^m}{\varepsilon} & \dfrac{\Phi_R^m(b_{R2}+\varepsilon)-\Phi_R^m}{\varepsilon} & \cdots & \dfrac{\Phi_R^m(b_{R66}+\varepsilon)-\Phi_R^m}{\varepsilon} \end{bmatrix} \tag{24}$$

where $\varepsilon = 10^{-6}$ is the small variation added to each kinematic parameter. For both methods, the J_I and J_R are of full rank which means all the internal and external kinematic parameters are identifiable.

The searching method of the optimal set of calibration configurations proposed by Nubiola et al. is used in this article to maximize the index O.[39] For both calibration methods, the numerical algorithm starts with a candidate set of 13 random configurations selected from the determined actuator stroke in the previous subsection. At each iteration, one configuration chosen from 5000 random configurations in the proper actuator stroke is added to the candidate group. If the index increases, we keep this configuration in the candidate group and remove any configuration which decreases the index of the set of configurations remaining, otherwise we remove this configuration and go to the next iteration.

Table 1. The standard deviations of the noise distribution.

	Standard deviation
Joint angle measurement (κ)	0.2233 bit
Pose measurement (x, y, z)	0.0096 mm
Pose measurement (β, γ, α)	0.0261°

Table 2. The standard deviations of the parameter errors distribution.

	Standard deviation
$[b_{l1}, b_{l2}, \ldots, b_{l48}]$	1 mm
$[b_{l49}, b_{l50}, \ldots, b_{l54}]$	0.00005 rad/bit
$[b_{l55}, b_{l56}, \ldots, b_{l60}]$	0.05 rad
$[b_{l61}, b_{l62}, b_{l63}], [b_{l67}, b_{l68}, b_{l69}]$	0.5 mm
$[b_{l64}, b_{l65}, b_{l66}], [b_{l70}, b_{l71}, b_{l72}]$	0.017 rad

For implicit calibration method, the algorithm is saturated after 618 iterations with the resultant index 0.0031 which cannot be improved. And for relative calibration method, the maximum index goes to 0.0322 with 572 iterations. The optimal sets for implicit and relative method contain 34 and 22 configurations, respectively.

Calibration simulation

In this subsection, the simulation is carried out on the case study of the posture variation of a 6-RSS parallel robot detected by the optical CMM system. The detection noise in the simulation is determined based on the experimental analysis.

As introduced in the previous section, the reflectors attached on the end-effector can be used as the feature points for the posture ${}^c\chi_t$ estimation. And the capturing noise of ${}^c\chi_t$ and joint angle measurements should be considered in the simulations. With a 10,000 times detection for the robot initial configuration, the error distribution of the feature points is obtained. Based on the results of noise analysis, the detection noise satisfies a two-dimensional normal distribution with standard deviations as shown in Table 1.

In the calibration simulation, we randomly generated a group of parameter errors $\mathbf{b}_I^n$, note that $\mathbf{b}_R^n$ is a subset of $\mathbf{b}_I^n$, complying with normal distribution. The standard deviations ρ given in Table 2 are roughly chosen such that a $\pm 3\rho$ error would lie in a $\pm 20\%$ of the nominal parameters.

In the simulation, the procedure of implementing the implicit calibration method is given as follows:

1. Load the initial parameters $\mathbf{b}_I^0$.
2. Generate a group of parameter errors with normal distributions of certain standard deviations as mentioned. By adding the errors to the initial parameters, we can obtain the real kinematic parameters $\mathbf{b}_I^n$.
3. Load the optimal set of 34 configurations derived from previous subsection for the implicit calibration method. Through equation (2), we convert the optimal set expression in the actuator domain into joint readings. Then we derive the joint measurement $\kappa^l (l = 1, ..., 34)$ by adding the detection noise to the joint readings.
4. The measurements of the poses ${}^c\chi_t^l$ are derived from the forward kinematics and equation (10), employing the real kinematic parameters $\mathbf{b}_I^n$. Also the detection noise should be added to the pose values.
5. The updating formula equation (11) is used to determine the optimal error parameters $\mathbf{b}_I$ by minimizing equation (12).

Table 3. The error norms between nominal and calibrated values—normal for implicit calibration method.

	Before calibration	After calibration
$\|\|\mathbf{b}_I^c - \mathbf{b}_I^n\|\|_2$	3.273	0.8197
$\sum_{l=1}^{34} \|\|\Phi_I^c - \Phi_I^n\|\|_2$	0.00109929	2.94235e−05

After 11 iterations, the calibrated error parameters $\mathbf{b}_I^c$ are found. The results with the norm of 72 error parameters and Φ_I are shown in Table 3.

For the RPBA simulation, the procedure is similar to that of the implicit calibration as follows:

1. Load the initial parameters $\mathbf{b}_R^0$.
2. Extract the subset $\mathbf{b}_R^n$ from $\mathbf{b}_I^n$.
3. Load the optimal set of 22 configurations derived and derive the joint measurement $\kappa^l (l = 1, ..., 22)$.
4. The measurements of the relative poses M^l are derived from the forward kinematics and equation (15), employing the real kinematic parameters $\mathbf{b}_R^n$. Also the detection noise should be added to the pose values.
5. The updating formula equation (17) is used to determine the optimal error parameters $\mathbf{b}_R$ by minimizing equation (18).

After four iterations, the calibrated error parameters $\mathbf{b}_R^c$ are found. The results with the norm of 66 error parameters and Φ_R are shown in Table 4.

Since the external parameters in b_c^χ representing the relationship between the sensor frame and the base frame are omitted in relative calibration method, we compare the two calibration methods using the criteria of relative accuracy10 which has widespread applications in industry field. The simulation procedure is given as follows:

1. Without loss of generality, a trajectory with 100 random relative configurations $M_n^l (l = 1, 2 \cdots 100)$ with respect to the initial configuration is generated.
2. Load the initial parameters $\mathbf{b}_I^u$, the calibrated parameters $\mathbf{b}_I^c$ and $\mathbf{b}_R^c$ are derived from the two calibration method.

3. Derive the trajectory expression in actuator domain θ_u^l, θ_I^l, and θ_R^l through the inverse kinematics and equation (15), employing $\mathbf{b}_I^u$, $\mathbf{b}_I^c$, and $\mathbf{b}_R^c$, respectively.
4. Input the deriving θ_u^l, θ_I^l, and θ_R^l into the real model of the robot separately, which employs the real parameters $\mathbf{b}_I^n$. Then we got three trajectories M_u^l, M_I^l, and M_R^l, respectively.

Table 4. The error norms between nominal and calibrated values—normal for RPBA.

	Before calibration	After calibration
$\|\|\mathbf{b}_R^c - \mathbf{b}_R^n\|\|_2$	3.1630	0.6616
$\sum_{l=1}^{22} \|\|\Phi_R^c - \Phi_R^n\|\|_2$	0.00542206	2.38881e–05

RPBA: relative posture-based algorithm

Converting M_n^l, M_u^l, M_I^l, and M_R^l into SE(3) space, we obtain χ_n^l (the nominal relative poses), χ_u^l (the relative poses deriving from uncalibrated parameters), χ_I^l (the relative poses deriving from implicit calibration result), and χ_R^l (the relative poses deriving from RPBA result), respectively. Then the pose errors $\chi_{u,e}^l$, $\chi_{I,e}^l$, and $\chi_{R,e}^l$ can be derived from $\chi_u^l - \chi_n^l$, $\chi_I^l - \chi_n^l$, and $\chi_R^l - \chi_n^l$ respectively.

The results are shown in Figure 6 and Table 5. The results show that the RPBA can improve the relative accuracy of the parallel robot in both translational and angular

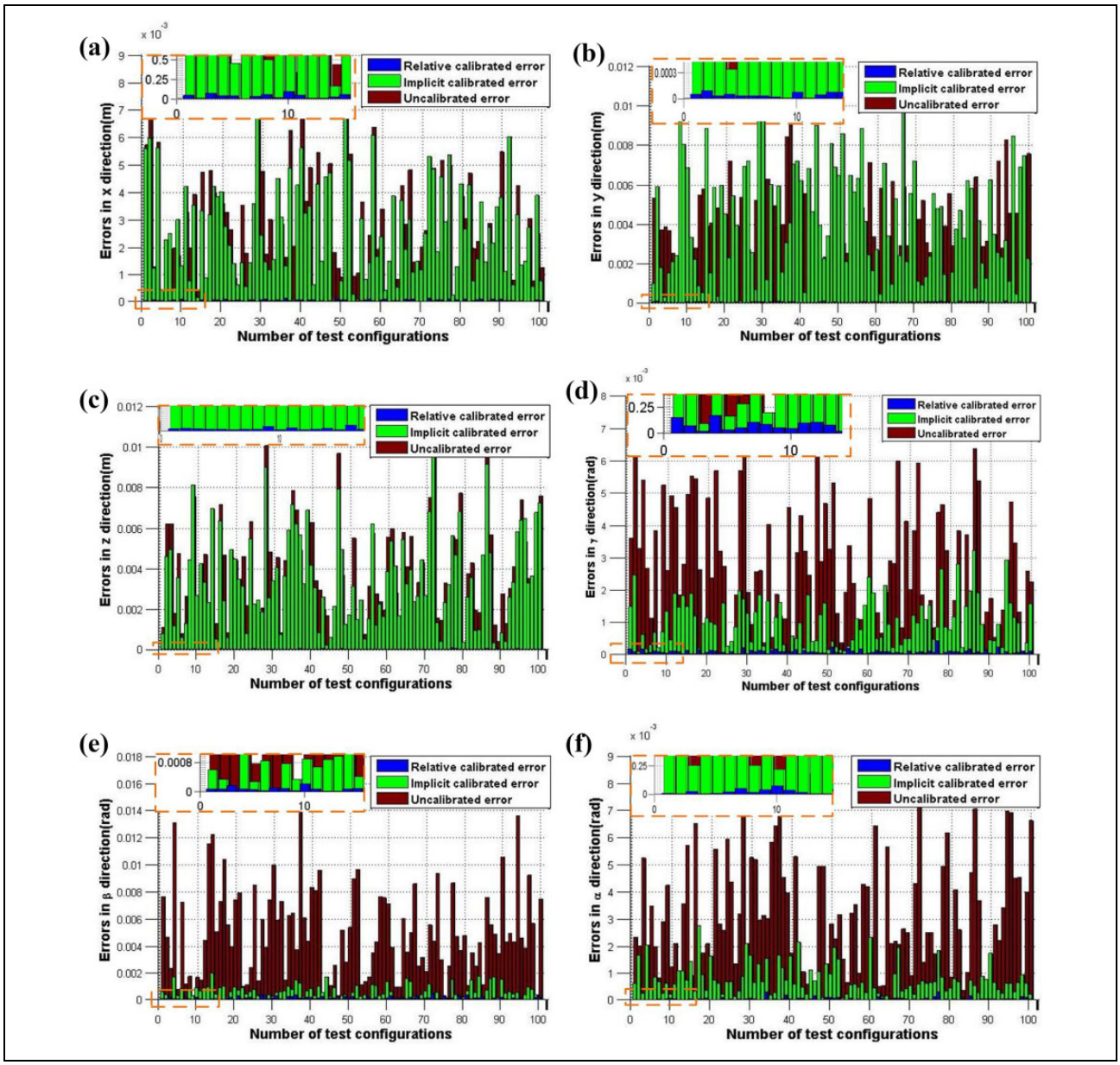

Figure 6. The simulation results of relative pose errors derived from implicit calibration, relative calibration, and uncalibration: (a) along *x* direction, (b) along *y* direction, (c) along *z* direction, (d) around α-axis, (e) around β-axis, (f) around γ-axis.

Table 5. The RMS of the relative pose errors in simulation.

	$\chi^{l}_{u,e}$	$\chi^{l}_{l,e}$ (mm)	$\chi^{l}_{R,e}$ (mm)
x (mm)	3.4	3.1	0.053
y (mm)	3.8	4.9	0.039
z (mm)	4.5	4.2	0.018
γ (rad)	0.0033	0.0012	9.7 e−5
β (rad)	0.0060	7.9 e−4	1.6 e−4
α (rad)	0.0037 *rad*	9.6 e−4	6.7 e−5

RMS: root mean square.

portions compared with the implicit calibration method. The implicit calibration results lead to a considerable improvement on the angular portion of the relative accuracy, but only slight improvement is gained in terms of the translational accuracy. The reason is that there are six more external parameters used in the implicit method. However, the relative accuracy is largely dependent on the internal parameters. The RPBA can improve the relative accuracy significantly in all directions of the relative pose along the given trajectory. Therefore, a conclusion can be drawn that considering the relative accuracy, the parallel robot can fulfill more accurate positioning tasks based on the proposed RPBA than those based on the implicit method.

Experimental verification

The experiment is supported by QUARC 2.1 platform (Quanser Inc., ON, Canada) which connects to the KEB-COMBIVERT motor servo through the interface card Sensory 626. The 6-RSS parallel robot is provided by Servo & Simulations Inc. (FL, USA) and two Quanser cards are used to communicate with six individual servers that deal with the dynamic control of actuators. One computer communicated with the optical CMM sensor C-Track 780 is in charge of image processing, and other computer deals with the control of the parallel robot. Serial port is used to transfer data between two computers. The experimental setup is shown in Figure 7.

As we can see, the base frame of the parallel robot is mechanical unaccessible and unobservable for the optical sensor. Since the manufacturer does not provide accurate geometric information, it is nontrivial and time-consuming to obtain a good initial guess of ${}^{c}\chi_{b}$. Thanks to the optical CMM, it allows us to derive the initial parameter of ${}^{c}\chi_{t}$ easily. Therefore, the RPBA is considered in this calibration experiment.

As shown in Figure 8, the reflectors are attached on the well-machined surface of the moving platform. Σe is designed on the symmetric center of the moving platform. At least three noncollinear points on each plane of plane A, plane B, and plane C are employed to build up equations of planes based on Cramer's rule. Then the intersection lines and points of three planes can be used to define the x direction of Σe, and the y direction is aligned with the norm of plane A. The original point of Σe is derived from the

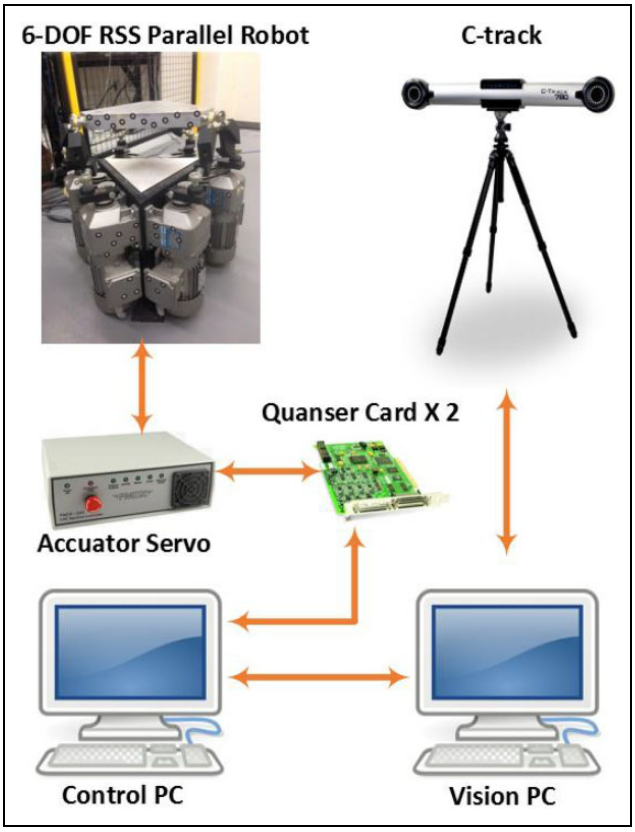

Figure 7. Experimental setup system.

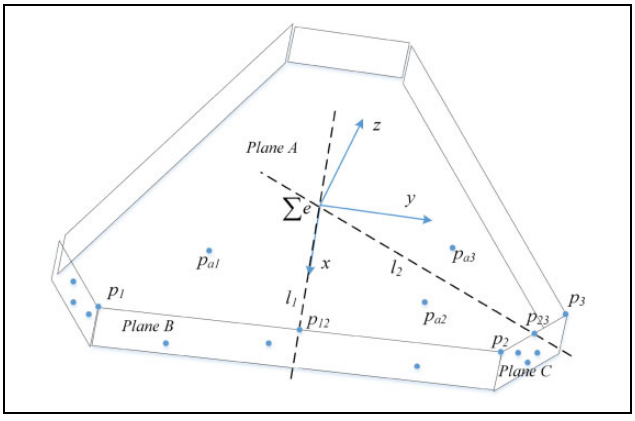

Figure 8. Measurement of ${}^{c}\chi_{t}$.

intersection point of l_1 and l_2. Then the derived Σe in the optical CMM sensor frame is directly used as the target frame. Therefore, the initial parameter of ${}^{c}\chi_{t}$ should be $[0,0,0,0,0,0]^{T}$.

For the relative calibration, the optimal set of 22 configurations derived from the previous section is selected as candidate configurations. And the actuator values are set as $[-60^{\circ},-60^{\circ},180^{\circ},180^{\circ},60^{\circ},60^{\circ}]$ for the initial configuration. At each configuration, the robot stops for 2 s and the sampling frequency of the potentiometer and C-track is 500 Hz and 29 Hz, respectively. The low-pass filters are used to

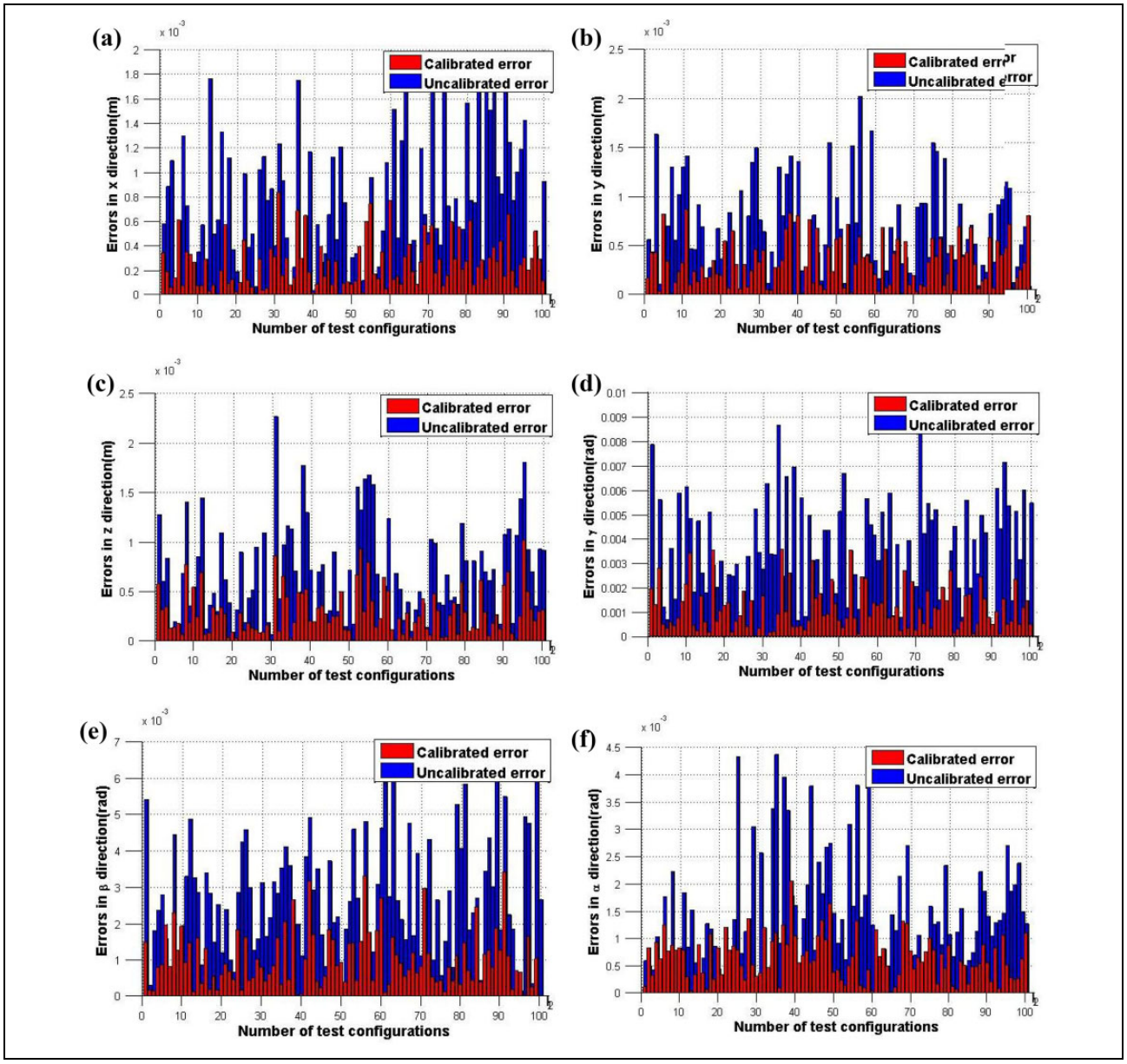

Figure 9. The experiment result of relative pose errors derived from calibrated model and uncalibrated model: (a) along the *x* direction; (b) along the *y* direction; (c) along the *z* direction; (d) around α-axis; (e) around β-axis; (f) around γ-axis.

remove the noise of the sensors, and the mean values are used for each configuration. Then the deriving ${}^{c}\chi_t^l$ and $\kappa^l(l = 0, 1 \cdots 22)$ are utilized in the objective function equation (17). Equation (18) is employed as the updating formula. After five steps iterations, the calibrated kinematic parameters are obtained. The objective function starts from 0.00155347 and converges to 7.07731e−05.

To verify the calibration results, a trajectory with 100 random relative configurations $\chi_n^l(l = 1, 2, \ldots, 100)$ with respect to its starting configuration inside the workspace of the parallel robot is chosen. And two trajectories are generated by the robot using uncalibrated and calibrated kinematic model, respectively. Also the mean values of the sensor reading are utilized in the experimental test. Using equation (15), the relative pose χ_c^l based on the calibrated kinematic model and χ_u^l based on the uncalibrated model can be derived. The pose errors after calibration $\chi_{c,e}^l$ should be $\chi_c^l - \chi_n^l$ and the pose errors before calibration $\chi_{u,e}^l$ can be derived from $\chi_u^l - \chi_n^l$. Those errors show how accurately the parallel robot can follow a given trajectory with respect to its starting point, which is also known as the relative accuracy of robots. The results are given in Figure 9 and Table 6. As we can see from the test results, the relative calibration can effectively improve the relative accuracy of the parallel robot on both translational and angular positioning. And this method is free from the tedious measurement of the relationship between the base frame and the sensor frame. It is concluded that the RPBA is an

Table 6. The RMS of the relative pose errors in experiment.

	Before calibration	After calibration
x (mm)	0.876	0.319
y (mm)	0.796	0.393
z (mm)	0.820	0.360
γ (rad)	0.039	0.0015
β (rad)	0.031	0.0013
α (rad)	0.017	7.464 e-04

RMS: root mean square.

implementable and effective method for the parallel robot calibration.

Conclusion

In this article, a relative posture-based kinematic calibration method is proposed for a 6-RSS parallel robot using the optical CMM system. The developed calibration algorithm can improve the positioning performance with respect to its initial configuration. In this algorithm, the base frame pose with respect to the sensor frame is not needed, which leads to an effective relative calibration method for the parallel robot. Since the forward kinematic model is used in the relative pose-based calibration, the optimal actuator strokes of the parallel robot are derived to ensure the homeomorphism mapping of the forward kinematic model. The simulation results show the relative pose-based calibration algorithm successfully improves the relative accuracy of the parallel robot. The comparison with the implicit calibration demonstrates that the RPBA can deliver a more satisfactory relative accuracy. The experimental tests on an arbitrary trajectory with 100 configurations further show that the proposed RPBA has improved the relative accuracy of the selected trajectories in 3-D space effectively. The developed calibration algorithm can be applied to other types of parallel and serial robots. And the calibration results would be used in a 6-RSS parallel robot visual servoing system in the future.

Declaration of conflicting interests

The author(s) declared no potential conflicts of interest with respect to the research, authorship, and/or publication of this article.

Funding

The author(s) received no financial support for the research, authorship, and/or publication of this article.

References

1. Wu J, Wang D, and Wang L. A control strategy of a two degrees-of-freedom heavy duty parallel manipulator. *J Dyn Syst Meas Control* 2015; 137: 061007.
2. Wu J, Yu G, Gao Y, et al. Mechatronics modeling and vibration analysis of a 2-dof parallel manipulator in a 5-dof hybrid machine tool. *Mech Mach Theory* 2018; 121: 430–445.
3. Journal I and Robotics OF. Overview of robot calibration. *IEEE J Robot Autom* 1987; 5: 377–385.
4. Wu L and Ren H. Finding the kinematic base frame of a robot by hand-eye calibration using 3d position data. *IEEE Trans Autom Sci Eng* 2017; 14: 314–324.
5. Wang D and Bai Y. Calibration of Stewart platforms using neural networks. In: *2012 IEEE conference on evolving and adaptive intelligent systems (EAIS)*, Madrid, Spain, 17–18 May 2012, pp. 170–175. IEEE.
6. Yu D, Li H, and Chen W. Kinematic calibration of parallel robots for docking mechanism motion simulation. *Int J Adv Robot Syst* 2011; 8: 47.
7. Wang L, Liu Y, Wu J, et al. Study of error modeling in kinematic calibration of parallel manipulators. *Int J Adv Robot Syst* 2016; 13: 1729881416672560.
8. Liu Y, Wu J, Wang L, et al. Kinematic calibration of a 3-dof parallel tool head. *Ind Robot: Int J* 2017; 44: 231–241.
9. Masory O, Wang J, and Zhuang H. Kinematic modeling and calibration of a Stewart platform. *Adv Robot* 1996; 11: 519–539.
10. Renaud P, Andreff N, Lavest JM, et al. Simplifying the kinematic calibration of parallel mechanisms using vision-based metrology. *IEEE Trans Robot* 2006; 22: 12–22.
11. Zhuang H. Self-calibration of parallel mechanisms with a case study on Stewart platforms. *IEEE Trans Robot Autom* 1997; 13: 387–397.
12. Abtahi M, Pendar H, Alasty A, et al. Experimental kinematic calibration of parallel manipulators using a relative position error measurement system. *Robot Comput Integr Manuf* 2010; 26: 799–804.
13. Hao Y, Changchun L, Xiaodong L, et al. Calibration of Stewart platform based on coordinate measurement. In: *Proceedings of international conference on modelling identification and control*, Shanghai, China, 26–29 June 2011, pp. 469–474. IEEE.
14. Besnard S and Khalil W. Calibration of parallel robots using two inclinometers. In: *Proceedings of the IEEE international conference on robotics and automation*, Detroit, MI, USA, 10–15 May 1999, vol. 3. pp. 0–5. IEEE.
15. Ibaraki S, Yokawa T, Kakino Y, et al. Kinematic calibration on a parallel kinematic machine tool of the Stewart platform by circular tests. In: *Proceedings of the American control conference*, Boston, MA, USA, 30 June–2 July 2004, vol. 2, pp. 1394–1399. IEEE.
16. Zhao L, Joubair A, Bigras P, et al. Metrological evaluation of a novel medical robot and its kinematic calibration. *Int J Adv Robot Syst* 2015; 12: 126.
17. Nubiola A, Slamani M, Joubair A, et al. Comparison of two calibration methods for a small industrial robot based on an optical CMM and a laser tracker. *Robotica* 2014; 32: 447–466.
18. Wampler CW, Hollerbach JM, and Arai T. An implicit loop method for kinematic calibration and its application to closed-chain mechanisms. *IEEE Trans Robot Autom* 1995; 11: 710–724.

19. Khalil W and Besnard S. Self calibration of Stewart–Gough parallel robots without extra sensors. *IEEE Trans Robot Autom* 1999; 15: 1116–1121.
20. Pradeep V, Konolige K and Berger E. Calibrating a multiarm multi-sensor robot: a bundle adjustment approach. In: *Springer tracts in advanced robotics*, vol. 79. Berlin, Heidelberg: Springer, pp. 211–225.
21. Daney D, Andreff N, Chabert G, et al. Interval method for calibration of parallel robots: vision-based experiments. *Mech Mach Theory* 2006; 41: 929–944.
22. Tan N, Clévy C, Laurent GJ, et al. Accuracy quantification and improvement of serial micropositioning robots for in-plane motions. *IEEE Trans Robot* 2015; 31: 1497–1507.
23. Hollerbach JM and Wampler CW. The calibration index and taxonomy for robot kinematic calibration methods. *Int J Robot Res* 1996; 15: 573–591.
24. Daney D. Choosing measurement poses for robot calibration with the local convergence method and tabu search. *Int J Robot Res* 2005; 24: 501–518.
25. Zeng R, Dai S, Xie WF, et al. Determination of the proper motion range of the rotary actuators of 6-RSS parallel robot. In: *2015 CCToMM symposium on mechanisms, machines, and mechatronics*, Carleton University, Ottawa, 28–29 May 2015, pp. 94–105. CCToMM.
26. Wang J and Masory O. On the accuracy of a Stewart platform. I. The effect of manufacturing tolerances. In: *Proceedings of the 1993 IEEE international conference on robotics and automation*, Atlanta, GA, USA, 2–6 May 1993, vol. 1, pp. 114–120. IEEE.
27. Mooring BW, Roth ZS, and Driels MR. *Fundamentals of manipulator calibration*. New York: Wiley, 1991.
28. Shirai Y. *Three-dimensional computer vision*. Berlin, Heidelberg: Springer Science & Business Media, 2012.
29. Hartley RI and Sturm P. Triangulation. *Comput Vis Image Understand* 1997; 68: 146–157.
30. Kanatani K, Sugaya Y, and Niitsuma H. Triangulation from two views revisited: Hartley–Sturm vs. optimal correction. *In Practice* 2008; 4: 5.
31. Wilson WJ, Hulls CCW, and Bell GS. Relative end-effector control using Cartesian position based visual servoing. *IEEE Trans Robot Autom* 1996; 12: 684–696.
32. Yuan JS. A general photogrammetric method for determining object position and orientation. *IEEE Trans Robot Autom* 1989; 5: 129–142.
33. Daniilidis K. Hand-eye calibration using dual quaternions. *Int J Robot Res* 1999; 18: 286–298.
34. Tan N, Gu X, and Ren H. Simultaneous robot-world, sensor-tip, and kinematics calibration of an underactuated robotic hand with soft fingers. *IEEE Access* 2017, PP(99), p.1.
35. Zeng R, Dai S, Xie W, et al. Constraint conditions determination for singularity-free workspace of central symmetric parallel robots. In: *IFAC-PapersOnLine* (eds A Dolgui, J Sasiadek and M Zaremba), vol. 28, pp. 1930–1935. Elsevier Ltd.: International Federation of Automatic Control.
36. Park FC and Kim JW. Singularity analysis of closed loop kinematic chains. *Trans ASME J Mech Des* 1999; 121: 32–38.
37. Bonev IA, Zlatanov D, and Gosselin CM. Singularity analysis of 3-DOF planar parallel mechanisms via screw theory. *J Mech Des* 2003; 125: 573.
38. Borm JH and Meng CH. Determination of optimal measurement configurations for robot calibration based on observability measure. *Int J Robot Res* 1991; 10: 51–63.
39. Nubiola A and Bonev IA. Absolute calibration of an ABB IRB 1600 robot using a laser tracker. *Robot Comput Int Manuf* 2013; 29: 236–245.